THE UNIVERSITY OF SCRANTON

BACHELOR OF SCIENCE THESIS

---

# Classical analogs for electromagnetically induced transparency

---

*Author:*
Joshua ZADOYKO

*Supervisor:*
Dr. Juan D. SERNA

*A thesis submitted in fulfillment of the requirements for the degree of B.S. in Physics*

*in the*

Research Group Name
Department of Electrical Engineering and Physics

April 25, 2018

# Declaration of Authorship

I, Joshua ZADOYKO, declare that this thesis titled, "Classical analogs for electromagnetically induced transparency" and the work presented in it are my own. I confirm that:

- This work was done wholly or mainly while in candidature for a research degree at this University.
- Where any part of this thesis has previously been submitted for a degree or any other qualification at this University or any other institution, this has been clearly stated.
- Where I have consulted the published work of others, this is always clearly attributed.
- Where I have quoted from the work of others, the source is always given. With the exception of such quotations, this thesis is entirely my own work.
- I have acknowledged all main sources of help.
- Where the thesis is based on work done by myself jointly with others, I have made clear exactly what was done by others and what I have contributed myself.

Signed:

Date:

*"Education is the most powerful weapon which you can use to change the world"*

Nelson Mandela

THE UNIVERSITY OF SCRANTON

# *Abstract*

Faculty Name
Department of Electrical Engineering and Physics

B.S. in Physics

**Classical analogs for electromagnetically induced transparency**

by Joshua ZADOYKO

This thesis explains the foundational concepts of electromagnetically induced transparency (EIT) in effort to develop a classical analog that will facilitate in the study of and comprehension of EIT. I show that there is a mathematical basis for which EIT behavior can be shown in both a coupled spring mass system and a coupled capacitor RLC circuit. It is demonstrated that the probe field can be modeled after the harmonic driving force or voltage signal, and the coupling field can be modeled after the coupling spring or coupling capacitor. This thesis also discusses a procedure for which both models can be done experimentally to prove the validity of the model.

# *Acknowledgements*

I gratefully acknowledge Dr. Juan Serna for his help with the development of my research and education.

# Contents

# List of Figures

*In loving memory of Michael Zadoyko*
*1963-2011*

# Chapter 1

# Introduction

Optical media have physical characteristics that allow light to be absorbed at certain frequencies. Imagine a scenario in which a beam of light tuned to a resonant frequency is absorbed by a medium. If a second beam of light is introduced and tuned to a resonant transition that shares a common energy level with the initial light source, the initial beam of light becomes transparent to the medium. This effect is a quantum interference phenomenon known as electromagnetically induced transparency (EIT) ([Har97]). EIT effects the dispersive properties of the medium, this includes low group velocity speeds of light propagating through the media ([Hau+99]), and the Kerr nonlinearity is largely enhanced [BHH13]. These effects have applications in, four wave mixing for the study of solitary-wave propagation ([AM86]), quantum memory for information storage and data processing ([NNS04]), and can be used as optical switches for fiber optics communication ([HH00]).

The term electromagnetically induced transparency was coined in a paper written in 1997 by S.E. Harris [Har97]. He showed that when a strong coupling field is driven to a resonant transition, the absorption of a weak probe field is eliminated. This assumes that the two resonant transitions carried out by the fields are coherently coupled to a common state [Har97]. The research carried out by Harris and his associates was demonstrated in a lambda-type energy level scheme with strontium gas vapor. Since then EIT has been explored in various optical mediums with varying configurations, as shown in figure 2.1. Recently, scientists have demonstrated that the "freezing of light" is possible, ultimately resulting in group velocity speeds as low as $17\,\mathrm{m/s}$ [Hau+99] for light propagating through media effected by EIT.

Classical analogs have been used and well documented to help scientists and students further understand quantum phenomena, examples of this are shown with the stimulated resonance Raman effect ([HP88]), time dependent Josephson phenomena ([SZ71]), adiabatic and non-adiabatic processes ([Mey79]), level repulsion ([FB94]), and coherent quantum states ([Wan17]). The examination and understanding of simple classical processes modeled by mathematical structures similar to the quantum ones facilitate the analysis and comprehension of these more complicated quantum counterparts.

As mentioned previously this thesis will be responsible for making a connection between a quantum phenomena and a classical system. The second chapter will be dedicated to describing EIT quantum mechanically, where I will develop the theory, discuss experimental results and applications of EIT. Chapter three will discuss the mathematical structures of two classical systems that are modeled closely to lambda-type EIT as driven damped harmonic oscillators. Chapter four will discuss the experimental procedures to obtain results that show EIT-like behavior in these two classical systems. The

fifth chapter will analyze the results of experiments I performed in both the spring-mass system and RLC circuit. The final chapter will discuss the conclusions I have drawn about the validity of these two classical systems representing behavior similar to that of EIT.

# Chapter 2

# Describing EIT Quantum Mechanically

This chapter will be responsible for outlining the key concepts for EIT as a quantum system, the applications of EIT, and a brief discussion of the experimental procedure for which EIT can be demonstrated. While the purpose of this thesis is to model the system classically, I feel that a brief description of the quantum system is helpful in order to see the connections between the quantum and classical worlds.

## 2.1 Theory

Our focus of this section will be directed on the theoretical structure of EIT in a three level system in the lambda-type configuration, but first I would like to give a brief description of EIT. A typical experiment for EIT consists of sweeping the probe field's frequency and recording the transmitted intensity of light traveling through the medium. This effect is dependent upon the condition that the coupling field is much stronger then the probe field, that is so the energy associated with the transition from states $|3\rangle \leftrightarrow |2\rangle$ (see Figure 2.1) is larger then all the damping rates present [Har97]. The effect of the coupling field is to induce a hyper-fine splitting of the excited state $|2\rangle$ so the probe field is now coupled to two indistinguishable states. This results in quantum interference of the coupled states, effecting the absorption profile of the probe field. In the absence of the coupling field a typical absorption profile is observed. The addition of the coupling field introduces a window of transparency as the probe field's frequency is swept near the resonant transition from states $|1\rangle \leftrightarrow |2\rangle$ (see Figure 2.1). The strength of the coupling field dictates how pronounced the window of transparency for the probe field is, and the resulting absorption spectrum becomes a doublet. This will be an important feature when we begin to establish a relationship between EIT and its classical analog.

The approach for the theoretical development of EIT can be done by following a semiclassical analysis, treating the laser fields classically, and modeling the atoms quantum mechanically. The optical response of an atom to resonant light is directly related to the complex susceptibility $\chi = \chi^{(1)} + i\chi^{(2)}$. The real part of the susceptibility $\mathrm{Re}[\chi]$ characterizes the refractive index of the media, and the imaginary part $\mathrm{Im}[\chi]$ describes the absorption of the field by the medium [FIM05]. The absorption coefficient is given by

$$\alpha = \frac{\omega_p n_0 \chi^{(2)}}{c}, \tag{2.1}$$

and the dispersion coefficient is given by

$$\beta = \frac{\omega_p n_0 \chi^{(1)}}{2c}, \tag{2.2}$$

where $n_0$ is the index of refraction and c is the speed of light [OM09].

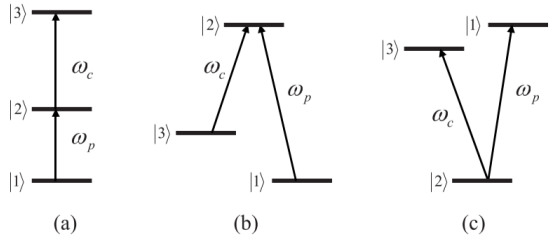


FIGURE 2.1: (a) ladder-type (b) lambda-type (c) V-type. The levels $|1\rangle$ and $|2\rangle$ are coupled by the probe field with frequency $\omega_p$, and levels $|2\rangle$ and $|3\rangle$ are coupled by the coupling field (also commonly referred to as the pump field) with frequency $\omega_c$. Only transitions $|1\rangle \leftrightarrow |2\rangle$ and $|2\rangle \leftrightarrow |3\rangle$ are dipole allowed. [OM09]

The susceptibility can be found by analyzing the density matrix of the three level system. The diagonal elements $\rho_{mn}$ give the probability that the system is in energy eigenstate n, and the off diagonal element describe the coherence between levels $n$ and $m$ [Boy03]. It can be shown that the off-diagonal elements of the density matrix are proportional to the induced electric dipole moment of the atom [[Man05]]. The time evolution of the density matrix can be found using the Liouville (Von Neumann) equation [SZ97]

$$\dot{\rho}_{nm} = -\frac{i}{\hbar}[\hat{H}, \hat{\rho}]_{nm} - \gamma_{nm}(\rho_{nm} - \rho_{nm}^{eq}). \tag{2.3}$$

Here the second term on the right hand of the equation is a phenomenological damping term, indicating that $\rho_{nm}$ relaxes to its equilibrium value $\rho_{nm}^{eq}$ at its decay rate $\gamma_{nm}$ [Boy03]. The effective Hamiltonian of the system is

$$H = \frac{\hbar}{2}\begin{bmatrix} 0 & \Omega_p & 0 \\ \Omega_p & -2\Delta_p & \Omega_c \\ 0 & \Omega_c & -2(\Delta_p - \Delta_c) \end{bmatrix}$$

with the probe field and coupling field represented as $\Omega_p$ and $\Omega_c$ respectively. The detuning from the $|1\rangle \leftrightarrow |2\rangle$ transition frequency $\omega_{12}$ and $\omega_p$ is given by $\Delta_p$. The detuning from the $|2\rangle \leftrightarrow |3\rangle$ transition frequency $\omega_{23}$ and $\omega_c$ is given by $\Delta_c$. In effort to model the EIT-lambda system the coupled differential equations of motion can be found by using Eq. 2.3 and the Hamiltonian given above in Eq. 2.1. The resulting equations are given below as

$$\dot{\rho}_{21} = ig_{21}E_p(\rho_{22} - \rho_{11}) + (i\Delta_p - \gamma_{21})\rho_{21} - ig_{32}E_c\rho_{32}, \tag{2.4a}$$
$$\dot{\rho}_{31} = ig_{21}E_p\rho_{32} + [i(\Delta_p - \Delta_c) - \gamma_{31}]\rho_{31} - ig_{32}E_c\rho_{21}, \tag{2.4b}$$
$$\dot{\rho}_{32} = ig_{21}E_p\rho_{31} - (i\Delta_c + \gamma_{32})\rho_{32} - ig_{32}E_c(\rho_{22} - \rho_{33}). \tag{2.4c}$$

The decay rates, $\gamma_{ij}$, are related to the natural decay rates of the states $\Gamma_{ij}$, by the relation $\gamma_{ij} = \frac{\Gamma_i + \Gamma_i}{2}$. The coupling and probe field amplitudes are denoted by $E_c$ and $E_p$, respectively. The dipole matrix elements for the transitions are $2\hbar g_{ij}$ and the Rabi frequency of the coupling laser is $\Omega_c = 2g_{32}E_c$ [OM09]. We are concerned with studying the characteristics of the probe laser, which is dictating the transition between the first and second energy level state. Solving the differential equations of motion from above, we get the following equations characterizing the coherence of the states as [FIM05]

$$\rho_{21} = \frac{-ig_{21}E_p e^{-i\omega_p t}}{(\gamma_{21} - i\Delta_p) + \frac{\Omega_c^2/4}{\gamma_{31} - i(\Delta_p + \Delta_c)}}, \tag{2.5a}$$

$$\rho_{31} = \frac{-ig_{32}E_c e^{-i\omega_c t}}{\gamma_{31} - i(\Delta_p - \Delta_c)}\rho_{21}. \tag{2.5b}$$

We can now begin to find the characteristics of the probe field subject to EIT. First we can relate the first order complex susceptibility to the polarization by Eq. 2.6a and the atomic polarization per unit volume by Eq. 2.6b [Boy03].

$$P = \frac{1}{2}\epsilon_0 E_p[\chi e^{-i\omega_p t} + c.c] \tag{2.6a}$$

$$P = -2\hbar g_{21} N \rho_{21} + c.c \tag{2.6b}$$

Combining both the equations above in Eq. 2.6 and incorporating the density matrix elements in Eq. 2.5 we can find the complex susceptibility written as

$$\chi = \frac{4i\hbar g_{21}^2/\epsilon_0}{(\gamma_{21} - i\Delta_p) + \frac{\Omega_c^2/4}{\gamma_{31} - i(\Delta_p + \Delta_c)}}. \tag{2.7}$$

With this information we can now take the Re[$\chi$] or the Im[$\chi$] and plug them into Eq. 2.2 and Eq. 2.1 respectively to determine the dispersion and absorption coefficients that characterize the medium as the probe field propagates through it.

## 2.2 Experimental Results

This section will briefly discuss the qualitative behaviors of an experimental demonstration of EIT. A quantitative comparison often becomes quite difficult due to the uncertainties that can arise in the frequencies of the coupling laser and the theoretical model discusses previously omits the hyperfine splitting that occurs in states due to the Stark effect. None the less qualitatively there is an agreement with the theoretical with the theoretical absorption profiles for low coupling laser power. What was not satisfied in the experimental results was the increasing or splitting of the window of transparency when a larger coupling field is present. While this is not immediately evident from these experimental results, it has been shown that an increase in the strength of the coupling field affects the splitting of the doublet, often referred to as the Aulter-Townes doublet. In the following chapter we will see that an increase in the coupling field which will be

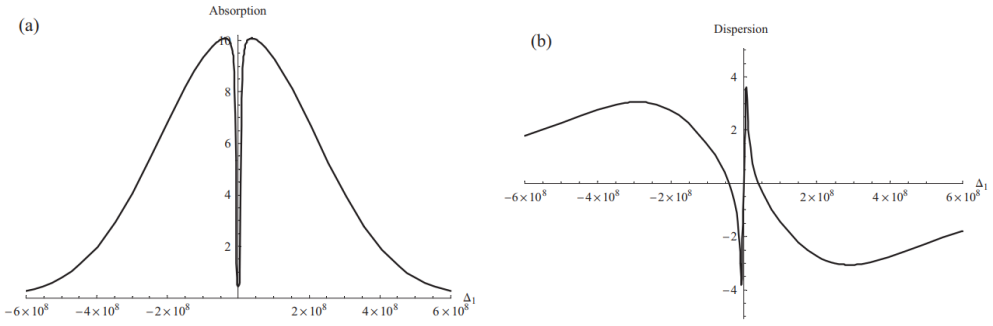


(a) (b)

FIGURE 2.2: Theoretical results for the absorption and dispersion of the probe beam. These results are obtained following a ladder-type EIT in rubidium. The $5S_{1/2} \rightarrow 5P_{3/2}$ transition serves as the probe transition at 780.2nm. The $5P_{3/2} \rightarrow 5D_{5/2}$ serves as the coupling transition at 776.0nm. [OM09]

modeled after the coupling spring or coupling capacitor will have a significant effect on the window of transparency.

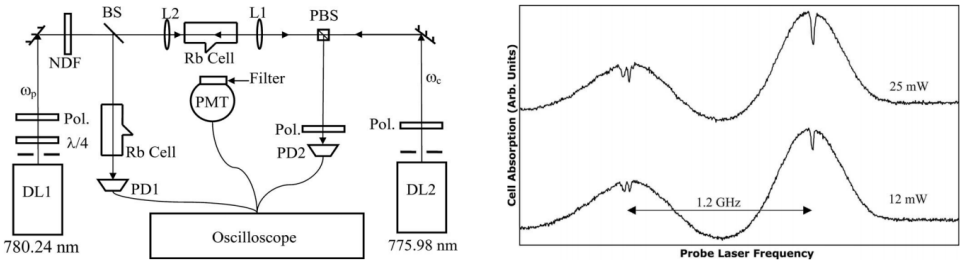


(a) (b)

FIGURE 2.3: (a) This is the experimental setup that can be used in order to perform EIT. (b) These are results of EIT where the 1.2GHz frequency span is the window of transparency for a rubidium gas. [OM09]

## 2.3 Applications

As previously discussed, EIT can be used to conduct much more complex phenomena because of the changes EIT places on the electromagnetic properties of a medium. Some of these applications were in, four-wave-mixing for the study of solitary-wave propagation ([AM86]), quantum memory for information storage and data processing ([NNS04]), and can be used as optical switches for fiber optics communication ([HH00]). In this section I will address how EIT can be used to aide in these phenomena.

The formation of Raman solitons are done when a four-wave-mixing phenomena occurs in a Raman medium. EIT concerns itself with the modifying Raman medium, changing the electromagnetic properties of the said medium. The medium requires

the existence of at least three energy states (0,1,2) where the highest-energy state (1) is coupled to the remaining two states (0,2), as seen in the EIT configuration in Fig. 2.1 [AM86]. The effects EIT has on this three level energy state system will be responsible for the study of solitary-wave propagation in Raman solitons via four-wave-mixing.

More recently, scientists have concerned themselves with quantum memory for information storage and date processing, and EIT is capable of aiding in this process. During EIT, the response of the quantum system to the probe field contains explicit information about its past states. In complex systems like three level lambda-type systems, the equations of motion can be used to study the memory of photons from their quantum states. During the coupling of states in EIT, a dark state is introduced which introduces long Rabi oscillations capable of storing and analyzing the past states of the system [AM86].

The final application I would like to mention is the use of EIT for optical switches and telecommunications, which actually utilizes a four-wave mixing technique that we discussed about previously. By using this four-wave mixing technique the implementation of dark resonance switching is possible (introduction of dark states). This switching is based on suppression and the enhancement of absorption for the fields in the four level system, which EIT is responsible for [HH00].

For a more in-depth discussion of these applications please see the cited sources, as this thesis' primary role is to discuss the learning of EIT through a classical analog and not to discuss EIT's role in applied physics.

# Chapter 3

# The Theory of EIT as a Mechanical Analogy

This chapter will be dedicated to studying the mathematical structures of a spring-mass system and coupled capacitor AC RLC circuit in effort to replicate the behavior exhibited in EIT.

As previously discussed, EIT is a technique for eliminating the effect a medium has on a propagating beam of light. The analog we can use to replicate this process for a spring mass system would simulate a driving force acting on a coupled spring mass system. Under the conditions for EIT, the driving force will become transparent to the mass as the driving frequency is swept near the mass' resonant frequency. If the coupled capacitor AC RLC circuit is to have EIT-like behavior we expect the AC signal to become transparent to the inductor of the first RLC loop, which will result in a negligible amount of power being absorbed by the inductor.

## 3.1 Driven Damped Harmonic Oscillators

Harmonic oscillators are found in almost any system that is displaced from equilibrium resulting in oscillations. If the only force acting on the system is a restoring force, the system is commonly referred to as a simple harmonic oscillator and only when the system introduces frictional forces the system can be classified as a damped oscillator. When a damped oscillator is displaced from equilibrium, the system will undergo oscillations, but any natural oscillator left to itself will eventually come to rest as the damping forces drain energy from the system. If one would like oscillations to continue, a external force must be applied in order for the system to not damp out. The system this thesis concerns itself with is the study of driven damped oscillators which are most often studied in AC driven RLC circuits and driven spring-mass systems. The equation of motion for a driven spring-mass system can be written as

$$m\ddot{x} + \gamma\dot{x} + kx = F(t), \tag{3.1}$$

where $\gamma$ is the frictional constant of proportionality, $k$ is the spring stiffness constant, and $F(t)$ is the external driving force. Similarly, the equation of motion for the circuit can be written as

$$L\ddot{q} + R\dot{q} + \frac{1}{C}q = \mathcal{E}(t), \tag{3.2}$$

where $L$ is the inductance, $R$ is the resistance, $C$ is the capacitance and $\mathcal{E}(t)$ is the external EMF signal. For now we will concern ourselves with the spring-mass system and seek a solution for Eq. 3.1. If we assume that are driving force is $f_0 e^{i\omega t}$, we will seek a solution in the form $Ae^{i\omega t}$ and find that this form will be a solution if and only if

$$A = \frac{f_0}{\omega_0^2 - \omega^2 + 2i\gamma\omega}. \tag{3.3}$$

From this result it can be observed that as the system evolves in time that the amplitude is effected by the frequency of the driving force. It can be shown that the maximum amplitude is reached when the frequency of the external force matches the frequency of the system, this phenomenon is known as resonance. If you look at the real part of the amplitude it is found that the maximum amplitude is given as

$$A_{max} \approx \frac{f_0}{2\gamma\omega_0}. \tag{3.4}$$

The concept of resonance will be a key feature as we begin to explore these coupled systems in the following sections and it will be shown that there is a dramatic change in behavior of these systems when modeled after EIT.

## 3.2 Mathematical Structure of a Coupled Spring-Mass System

We can begin to model lambda-type EIT as a system of coupled springs and masses. The two masses are coupled by a spring $K$ which we will relate to the coupling field. Springs $k_i$ ($i = 1, 2$) are connected to their respective masses and fixed to walls on opposite ends, which represents the transitions shared by a common energy level with frequencies $\omega_i$. Mass one will be subject to a driving force with amplitude $F_0$ and driving frequency $\omega_p$, acting as the probe field.

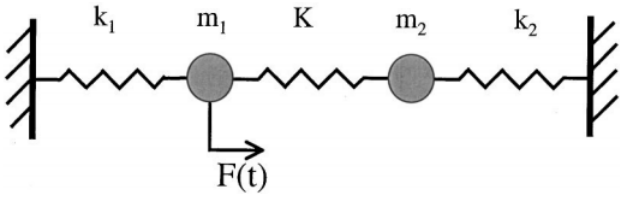


FIGURE 3.1: The spring mass model used to demonstrate EIT-like behavior. [AMN02]

Our goal will be to analyze the power that is transferred from the driving force to $m_1$. With the introduction of the coupling spring the expectation is that the absorption spectrum will contain features behaving like EIT. To provide a mathematical description of the system, the differential equations describing the evolution of $m_1$ and $m_2$ are

$$\ddot{x}_1 + 2\gamma_1\dot{x}_1 + \omega_1^2 x_1 - \Omega_1^2 x_2 = \frac{F_0}{m} e^{-i\omega_s t}, \tag{3.5a}$$

$$\ddot{x}_2 + 2\gamma_2\dot{x}_2 + \omega_2^2 x_2 - \Omega_2^2 x_1 = 0. \tag{3.5b}$$

Here we choose springs $k_i$ to be similar in strength, which models closely to lambda-type EIT. The frequency of the coupled masses are given as $\Omega_i = \sqrt{K/m_i}$, and frictions constants $\gamma_1$ and $\gamma_2$ model the energy dissipation of $m_1$ and $m_2$ respectively, relating to spontaneous and stimulated emission of the three level system. Since we are seeking the amount of power absorbed from $m_1$ by the driving force, we seek a solution for $x_1(t)$ and assume it in the form of $Ne^{-i\omega t}$ and assume $x_2(t)$ takes a similar form. Substituting the assumed solutions for the positions of $m_1$ and $m_2$ in Eq. 3.5, the position of $m_1$ is found to be

$$x_1(t) = \frac{F_0(\omega_2^2 - \omega_s^2 - i\gamma_2\omega_s)}{m\left[(\omega_1^2 - \omega_s^2 - i\gamma_1\omega_s)(\omega_2^2 - \omega_s^2 - i\gamma_2\omega_s) - \Omega_1^2\Omega_2^2\right]} e^{-i\omega_s t}. \tag{3.6}$$

Using Eq. 3.6, the absorbed power from the driving force by mass one during one period of oscillation is

$$P(\omega_s) = \frac{1}{T}\int_0^T F_0 e^{-i\omega_s t}\dot{x}_1 dt \tag{3.7}$$

$$= \frac{2\pi i F_0^2 \omega_s(\omega_2^2 - \omega_s^2 - i\gamma_2\omega_s)}{m\left[(\omega_1^2 - \omega_s^2 - i\gamma_1\omega_s)(\omega_2^2 - \omega_s^2 - i\gamma_2\omega_s) - \Omega_1^2\Omega_2^2\right]}, \tag{3.8}$$

It is demonstrated in Fig **??** that a window of transparency is observed as the detuning between the driving force and the natural frequency of $m_1$ approaches zero. The separation of the doublet becomes more pronounced as the coupling spring becomes more stiff as predicted in the theoretical development of this analog.

## 3.3 Mathematical Structure of a Coupled Capacitor RLC Circuit

Much like the spring-mass system that we previously described, a similar behavior can be demonstrated when observing a coupled capacitor RLC circuit driven by an AC signal. The electrical analog to the system in Fig. **??** is the circuit shown in Fig. **??**, where the first mesh with $L_1$ and $C_1$ and coupling capacitor $C$ model the coupling field and $R_1$ models the losses associated with this oscillator. The second mesh with $L_2$, $C_2$ and $C$ model the transition between states $|1\rangle$ and $|2\rangle$ and $R_2$ models the spontaneous decay from the excited state that couples the fields (state 2). The coupling capacitor $C$ that involves both meshes, models the coupling of the transitions between the states. Finally, it is the AC signal $V_s$ that models the probe field with a tunable frequency $\omega_s$.

In effort to replicate the behaviors exhibited in EIT we look to find the power that is transferred from the voltage signal $V_s(\omega_s)$ to the inductor in the second mesh, labeled $L_2$. We can begin to model this system with these coupled differential equations for the charges in each loop as

$$\ddot{q}_1 + \gamma_1\dot{q}_1 + \omega_1^2 q_1 - \Omega^2 q_2 = 0, \tag{3.9a}$$

$$\ddot{q}_2 + \gamma_2\dot{q}_2 + \omega_2^2 q_2 - \Omega^2 q_1 = \frac{V_0 e^{i\omega t}}{L_2}. \tag{3.9b}$$

In this case $\gamma_i = R_i/L_i$ (i=1,2), $\omega_i^2 = 1/(L_i C_{ei})$ ($C_{ei}$ is the series combination of the coupling capacitor and the capacitor in the respective mesh loop), and $\Omega^2 = 1/(L_2 C)$.

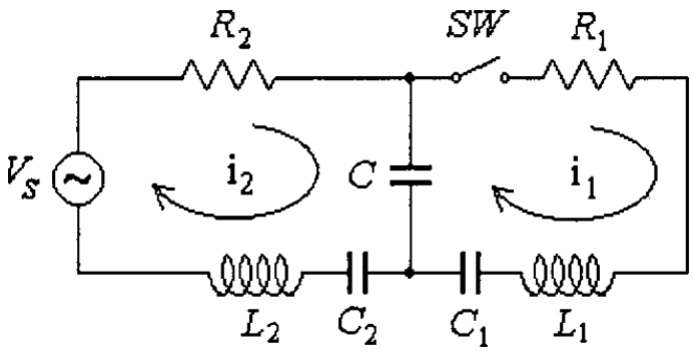


FIGURE 3.2: The electrical circuit used to study EIT-like behavior. [AMN02]

The equivalent capacitances for these loops are given as a series combination in the form

$$C_{e1} = \frac{CC_1}{C + C_1} \tag{3.10a}$$

$$C_{e2} = \frac{CC_2}{C + C_2} \tag{3.10b}$$

Next, by applying Kirchhoff's second law to the two loops of the circuit with the currents defined in each mesh $I_1$ and $I_2$ as seen in Fig. **??**, we obtained

$$j\, I_1 X_C + I_2 \left(R_2 - \mathrm{i}\left(X_C + X_{C_2} - X_{L_2}\right)\right) = V_s \tag{3.11a}$$

$$\mathrm{i}\, I_2 X_C + I_1 \left(R_1 - \mathrm{i}\left(X_C + X_{C_1} - X_{L_1}\right)\right) = 0 \tag{3.11b}$$

where $X_C = 1/\omega_i C$ and $X_{C_i} = 1/\omega_i C_i$ are the impedances associated with the capacitors and $X_{L_i} = \omega L_i$ are the impedances of the inductors in the circuit. From the above system of equations it is found that the the current in the second loop is defined as:

$$I_2 = \frac{(X_C + X_{C_1} + X_{L_1} + \mathrm{i}R_1)(A + \mathrm{i}B)}{A^2 + B^2} V_0 \tag{3.12}$$

where $A$ and $B$ were written for convenience, defined as

$$A = R_2\left(X_C + X_{C_1} - X_{L_1}\right) + R_1\left(X_C + X_{C_2} - X_{L_2}\right), \tag{3.13a}$$

$$B = \left(X_{C_1} - X_{L_1}\right)\left(X_{C_2} - X_{L_2}\right) + X_C\left(X_{C_1} + X_{C_2} - X_{L_1} - X_{L_2}\right) - R_1 R_2. \tag{3.13b}$$

The electrical power in the second loop was obtained by multiplying Eq. 3.12 by the voltage amplitude from the voltage source, resulting in the following expression:

$$P = \frac{(X_C + X_{C_1} + X_{L_1} + \mathrm{i}R_1)(A + \mathrm{i}B)}{A^2 + B^2} V_0^2 \tag{3.14}$$

insert graphs here.

# Chapter 4

# Experimental Design of the Mechanical Analogy

This chapter will be dedicated to describing how these models can be performed experimentally, in effort to validate the claim that the mechanical analogs are in fact able to have EIT-like behavior in their respective physical systems.

## 4.1 Spring-Mass System Experiment

This experiment can be performed by analyzing the power transfered from the external driving force to the first mass in the system. The system we will use is a rectilinear control plant made by Educational Control Products. This system has the capabilities of driving a system of springs and masses with a variety of functions, more importantly, it has the ability to apply a sinusoidal forcing at a range of frequencies. This section will first discuss the measurements and analysis performed in order to measure the physical parameters of the system and discuss the experimental procedure that can be carried out using this control plant in effort to model EIT-like behavior.

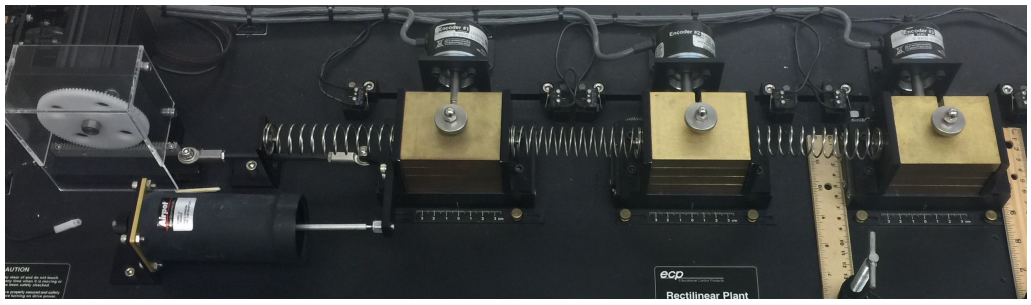


FIGURE 4.1: This is the spring mass setup I use as my classical analog to EIT with $m_1$ being driven by the control system (left), $m_2$ being coupled by the spring attached to $m_1$ (middle) and the right most spring is attached to a fixed wall (right most body acts as a wall).

### 4.1.1 Determining Parameters

A few experiments must be performed in preparation for observing EIT-like phenomena with masses and springs. This includes measurements for the spring coefficients, determining the damping coefficients for both masses and address the precision of the

control plants driving frequency. The measurements of the spring constants will be done by utilizing Hooke's law and then verified by measuring the period of oscillation for the spring as a simple harmonic oscillator. The damping coefficients will be determined by analyzing their behavior using a fitting algorithm under the assumption the system can be modeled as a damped harmonic oscillator.

FIGURE 4.2: Apparatus for measuring the spring coefficients for all of the springs used ($k_1$,$k_2$, and $K$) in this experiment.

The spring coefficients were found using the experimental setup seen in Fig. 4.2. Each spring was hung vertically on the top of the apparatus and then additional weight was attached to the bottom of the spring. As their is more weight added to the spring, it will be stretched and be displaced from equilibrium. Hooke's law states that the force exhibited on the spring is proportional to the displacement of the spring. If the displacement of the mass is plotted in the x-axis and the force of gravity ($M_{total} * g$) in the y-axis, the linear fit of this line gives a good approximation for the three springs constants we wish to determine. To verify these results with a more accurate method we can displace the mass from equilibrium and obserrve the oscillatory motion of the mass. The relationship between the period of oscillation and the spring constant is

$$k = 4\pi^2 \frac{(M + \frac{m_s}{3})}{T^2}, \tag{4.1}$$

where $T$ is the period of oscillation, $M$ is the mass attached to the spring, and $m_s$ is the mass of the spring. Listed below are the results for each spring, note that the results for each spring was calculated as an average of three individual experiments for both the Hooke's law and period of oscillation method.

| Spring constants | | |
|---|---|---|
| Spring | Hooke's Law method | Period of oscillation method |
| $k_1$ | $402.34 \pm 17.77\,\mathrm{N/m}$ | $415.49 \pm 0.37\,\mathrm{N/m}$ |
| $k_{12}$ | $198.85 \pm 9.19\,\mathrm{N/m}$ | $204.48 \pm 0.25\,\mathrm{N/m}$ |
| $k_2$ | $381.51 \pm 18.99\,\mathrm{N/m}$ | $381.88 \pm 0.68\,\mathrm{N/m}$ |

These results are quite satisfying in the fact that all the measurements with their respective uncertainties are in agreement with each other. For the purposes of this experiment we will consider using the spring coefficients calculated from the period of oscillation method when comparing the physical system to the theoretical models developed in the previous chapter.

The damping coefficients of each mass were found when each mass spring system was treated as a damped harmonic oscillator displaced from its equilibrium position and then released from rest. Each position vs time graph was fitted using the Scaled Levenberg-Marquardt algorithm with the solution for a damped harmonic oscillator

$$x_i(t) = A\cos(\omega_i t + \delta_i)e^{-i\gamma_i t}, \tag{4.2}$$

where $A$ is the amplitude, $\omega_i$ is the natural frequency of oscillation, $\gamma_i$ is the damping coefficient, and $\delta_i$ is the phase shift. The velocity dependent damping coefficients were found to be $\gamma_1 = 2.42$ and $\gamma_2 = 0.54$ and the fits for those curves are shown in Fig. **??**.

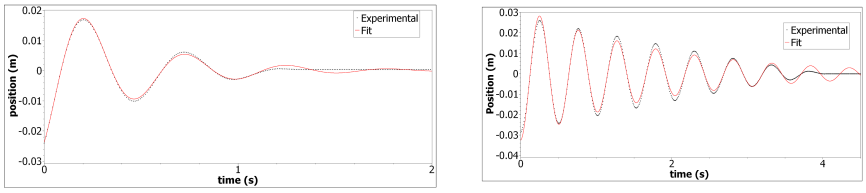


(a) (b)

FIGURE 4.3: Experimental fits for finding damping parameters of the system, (a) experimental fit with the $m_1$ attached to a damping dashpot (used to increased velocity dependent damping), and (b) experimental fit for $m_2$.

The last item to consider was the accuracy of the forcing frequency (given in Hz) which was considered to be as accurate as $\pm 0.2$ hertz. This was determined by viewing data from the control plant for varying frequencies and observing the period between consecutive peaks.

The final information is provided by the educational control plant datasheet, listing the mass of each carriage as $m_{c1} = 0.56\,\text{kg}$, and the mass of carriage 2 as $m_{c2} = 0.72\,\text{kg}$. Additional weight can be placed on the carriages that totals up to 2 kg. With this data we can now see the expected results of our spring mass analog by applying Eq. 3.7 under these newly determined parameters, as seen in Fig. **??**.

### 4.1.2 Experimental Procedure

This experiment can be performed in an iterative process, setting the forcing frequency to values at and near the resonant frequency of mass one $\omega_1$ and then calculating the average power over $n$ periods of oscillation. The data acquisition system from the rectilinear control plant provides us with the velocity at time t, with this, it is possible to calculate the average power transferred to the mass being forced over one period of oscillation. As mentioned previously, this process will be repeated until enough points have been found to make conclusions of the frequency dependence of the absorption profile and the window of transparency becomes apparent.

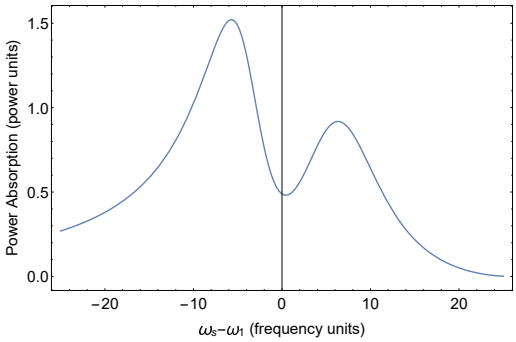


FIGURE 4.4: Theoretical graph of EIT classical analog using determined parameters.

It can be seen directly from the position vs time graph if EIT is being observed, under the condition that as the driving frequency nears $\omega_1$, the amplitude of the mass should be decreasing. This can be stated because under the theory of EIT as this detuning approaches zero, the driving force becomes "transparent" to the mass, hence a negligible amount of power has been transferred from the external driving force to the mass in a constructive manner, resulting in low amplitudes of the oscillatory motion.

## 4.2 RLC Circuit Experiment

This experiment can be performed by analyzing the power transfered from the AC voltage signal to the second mesh loop as seen in Fig. **??**. In effort to find the power transferred into the second mesh as the frequency is swept through resonance, the circuit was soldered onto a protoboard. Much like the spring-mass experiment, this experiment will also be done in an iterative process, where as the AC signal's frequency is swept, the current running through the second mesh is being measured and an EIT window of transparency should be demonstrated for the driven coupled capacitor RLC circuit.

This section will discuss experimental procedure that can be carried out using this circuit in effort to model EIT-like behavior.

### 4.2.1 Experimental Procedure

This experiment can be performed in an iterative process that resembles closely to the experimental procedure for the spring-mass system that was discussed previously. As previously mentioned, our goal will be to analyze the power that is being transferred from the AC voltage signal to the second mesh of the coupled RLC circuit. To carry out this procedure we will sweep through a range of frequencies and pass through the resonant frequency while simultaneously measuring the current that is passing through the second mesh labeled $i_2$ in Fig. **??**. As we begin to sweep through the resonant frequency we expect to observe a local minima at or near the resonant frequency of the second mesh and two local maximas shifted away from the resonant frequency, creating the doublet we saw previously that characterized the EIT window of transparency.

Originally the circuit was intended to be tested on a bread board, but due to stability and fluctuations with the readings it was determined that this experiment might be best

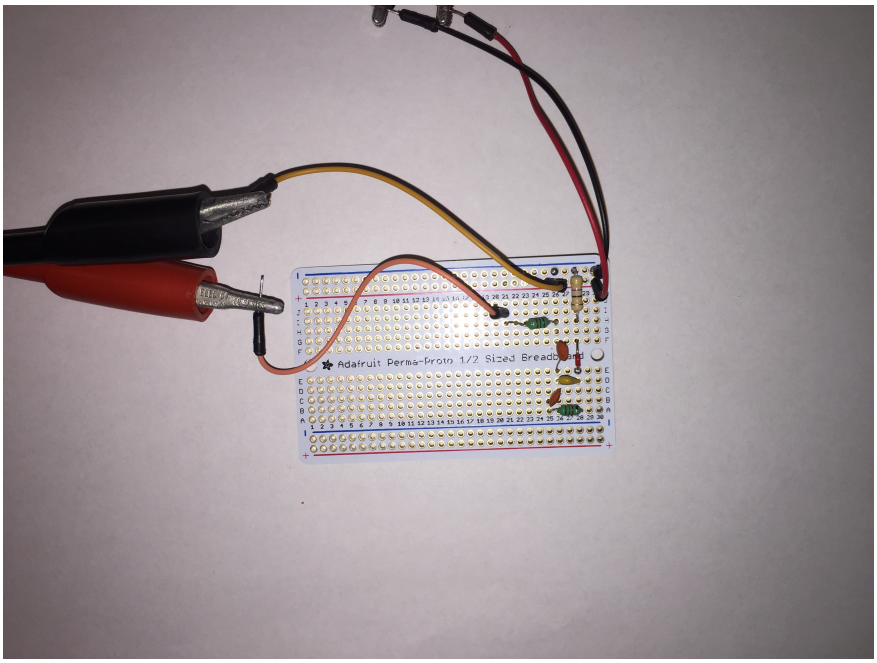


FIGURE 4.5: This is the circuit that was used to model lambda-type EIT. The orange cables are connected in order to measure the current going through the second mesh and the black and red leads supply the power to the circuit. For this experiment we used the following values, $C_1 = 0.102\mu\,\mathrm{F}$, $C_2 = 0.084\mu\,\mathrm{F}$, $C = 0.198\mu\,\mathrm{F}$, $L_1 = 0.934\,\mathrm{mH}$, $L_2 = 0.929\,\mathrm{mH}$, $R_2 = 50\Omega$ and $R_1 = 0\Omega$.

suited to be done with soldered components. Additional equipment will be required for this experiment which consists of a wave generator, preferably having the ability to sweep through frequencies ranging from 0 to 1 MHz and capable of supplying a voltage of 20V Pk-Pk. The final piece of equipment that will be necessary is a ammeter (capable of support the voltage being fed into the circuit) that can detect differences in current up to $1\mu$ A. It will also be helpful to have an oscilloscope at hand to make verify that the AC signal is properly supplying the desired signal into the circuit.

On a final remark for students who wish to recreate these results, when deciding components that you would like to use, it is important to remember that picking components with approximately the same values and of the same order will make the data analysis much more apparent. On another note remember that when the coupling capacitor value gets considerably smaller compared to the other capacitor values in the circuit, the window of transparency that is to be viewed occurs over a much narrower region of frequencies and will require a reliable, high precision wave generator and ammeter to get the desired results.

# Chapter 5

# Results and Analysis

## 5.1 Spring-Mass System

It is observed in Fig. **??** that the detuning frequency for which the most absorption occurs has shifted. The different masses and springs used in this experiment may be a result of the asymmetry observed. My conclusion is that this shift is the result of the natural frequency of oscillation for $m_1$ is now expressed as $\omega_0 = \sqrt{\omega_1^2 - \gamma_1^2}$. This result is still satisfying in the fact that we see a doublet similar to what we saw in Fig. **??**, and a significant amount of absorption occurs as the detuning between the natural frequency of oscillation for mass one and the driving force approaches zero.

At this time I have still been unsuccessful of obtaining results similar to Fig. **??**, these are the observations I have made in attempt to solve this issue. Thus far I have considered a harmonic forcing in the form $F_0 * e^{-i\omega_s t}$, in this experiment I am restricted to a sinusoidal forcing $F_0 \sin(\omega_s t)$. Another factor I have neglected thus far for simplicity of solving the coupled differential equations is the two types of frictions present, a linear $sgn(\vec{v})$ dependent damping and the velocity dependent damping. For simplicity these two were combined into the $\gamma_i$ coefficients, experimentally these two should be considered independently, which will now present a discontinuity in the differential equations. The differential equations describing the motion of the masses is now written as

$$\ddot{x}_1 + 2\gamma_1\dot{x}_1 + \omega_1^2 x_1 - \Omega_1^2 x_2 - \mu_{k1} N_1 \operatorname{sgn}(\dot{x}_1) = \frac{F_0}{m}\sin(\omega_s t), \tag{5.1a}$$

$$\ddot{x}_2 + 2\gamma_2\dot{x}_2 + \omega_2^2 x_2 - \Omega_2^2 x_1 - \mu_{k2} N_2 \operatorname{sgn}(\dot{x}_2) = 0, \tag{5.1b}$$

where $N_i$ is the normal force, $\mu_{ki}$ is the coefficient of friction between track and carriage, and the $\operatorname{sgn}(\dot{x}_i)$ is $-1$ when the velocity is negative, and 1 when the velocity is positive. As previously mentioned this creates a discontinuity which will require a numerical solution to the differential equations. I will continue to explore different avenues for approaching the desired results. At this point in time I am still observing a typical absorption spectrum with the coupled spring mass setup seen in Fig 4.1.

## 5.2 AC RLC Circuit

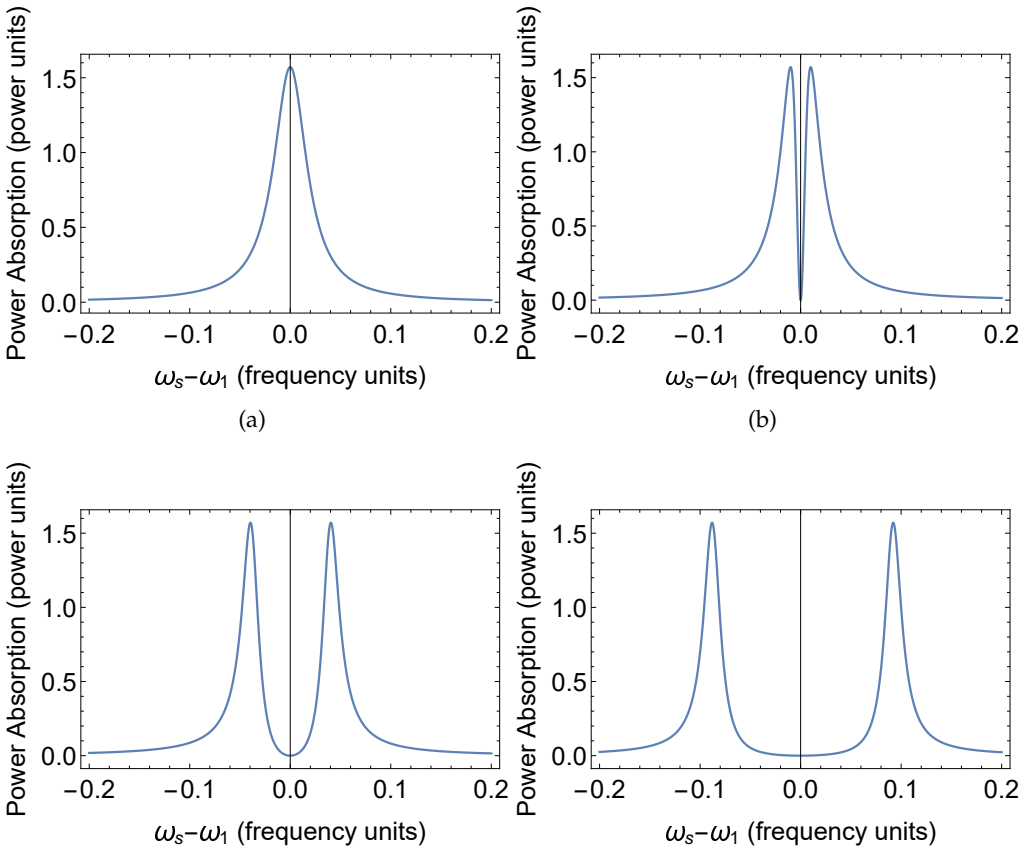


FIGURE 5.1: The dependence of the absorption based on the frequency of the driving force. The values used are $m_1 = m_2 = 1$, $\omega_1 = \omega_2 = 1.0$, $\gamma_1 = .004$, $\gamma_2 = 10^{-7}$, and $F_0 = 0.1$. The values for the coupling frequency are $\Omega_1 = \Omega_2$, (a) 0.0, (b) 0.2, (c) 0.4, (d) 0.6 in units of .

## Chapter 6

# Conclusions

Classical analogs can be a useful tool in understanding systems that are very complex or abstract. They allow for the interpretation of behavior that can be explained much more easily as a classical system without having to understand the complex nature of atomic systems. On the other hand they have their differences, and that always must be considered when making the relationship between quantum and classical systems.

Thus far I have established a classical analog to EIT as a spring mass system and shown in theory that it does in fact model behavior shown in the quantum system. We have seen first hand the frequency dependence of the probe field in the absorption spectrum, and have seen the relationship between the strength of the coupling field and the splitting of the doublet. Unfortunately I have been unsuccessful in proving this theory in practice and I will continue to explore different avenues to approach these theoretical results.

# Bibliography


[AM86] Jay R. Ackerhalt and Peter W. Milonni. "Solitons and four-wave mixing". In: *Phys. Rev. A* 33 (5 1986), pp. 3185–3198. DOI: 10.1103/PhysRevA.33.3185. URL: https://link.aps.org/doi/10.1103/PhysRevA.33.3185.

[AMN02] C. L. Garrido Alzar, M. A. G. Martinez, and P. Nussenzveig. "Classical analog of electromagnetically induced transparency". In: *American Journal of Physics* 70.1 (2002), pp. 37–41.

[BHH13] Zhengyang Bai, Chao Hang, and Guoxiang Huang. "Classical analogs of double electromagnetically induced transparency". In: *Optics Communication* 291 (2013), pp. 253–258.

[Boy03] Robert W. Boyd. *Nonlinear Optics*. Academic Press, 2003, pp. 129–175.

[FB94] Winfried Frank and Peter V. Brentano. "Classical analogy to quantum mechanical level repulsion". In: *American Journal of Physics* 62 (1994).

[FIM05] Michael Fleischhauer, Atac Imamoglu, and Jonathan P. Marangos. "Electromagnetically induced transparency: Optics in coherent media". In: *Rev. Mod. Phys.* 77 (2 2005), pp. 633–673. DOI: 10.1103/RevModPhys.77.633. URL: https://link.aps.org/doi/10.1103/RevModPhys.77.633.

[Har97] Stephen E. Harris. "Electromagnetically Induced Transparency". In: *Physics Today* (1997).

[Hau+99] Lene Vestergaard Hau et al. "Light speed reduction to 17 metres per second in an ultracold atomic gas". In: *Nature* 397 (1999), pp. 594–598.

[HH00] Byoung S. Ham and Philip R. Hemmer. "Coherence Switching in a Four-Level System: Quantum Switching". In: *Phys. Rev. Lett.* 84 (18 2000), pp. 4080–4083. DOI: 10.1103/PhysRevLett.84.4080. URL: https://link.aps.org/doi/10.1103/PhysRevLett.84.4080.

[HP88] P. R. Hemmer and M. G. Prentiss. "Coupled-pendulum model of the stimulated resonance Raman effect". In: *J. Opt. Soc. Am. B* 5.8 (1988), pp. 1613–1623. DOI: 10.1364/JOSAB.5.001613. URL: http://josab.osa.org/abstract.cfm?URI=josab-5-8-1613.

[Man05] Kim Dae Mann. *Introduction to Quantum Mechanics for Applied Nanotechnology*. John Wiley and Sons Inc., 2005, pp. 167–187.

[Mey79] Hans-Dieter Meyera. "A classical analog for electronic degrees of freedom in nonadiabatic collision processes". In: *The journal of chemical physics* 70 (1979).

[NNS04] A. Nazarkin, R. Netz, and R. Sauerbrey. "Electromagnetically Induced Quantum Memory". In: *Phys. Rev. Lett.* 92 (4 2004), p. 043002. DOI: 10.1103/PhysRevLett.92.043002. URL: https://link.aps.org/doi/10.1103/PhysRevLett.92.043002.

[OM09] Abraham J. Olson and Shannon K. Mayer. "Electromagnetically induced transparency in rubidium". In: *American Journal of Physics* 77.2 (2009), pp. 116–121. DOI: 10.1119/1.3028309. eprint: https://doi.org/10.1119/1.3028309. URL: https://doi.org/10.1119/1.3028309.

[SZ71] D. B. Sullivan and J. E. Zimmerman. "Mechanical Analogs of Time Dependent Josephson Phenomena". In: *American Journal of Physics* 39 (1971).

[SZ97] Marlan O. Scully and M. Suhail Zubairy. *Quantum Optics*. Cambridge U.P., 1997.

[Wan17] Dong-Sheng Wang. "Strong Analog Classical Simulation of Coherent Quantum Dynamics". In: *Communications in Theoretical Physics* 67 (2017).